Title

Computer-Assisted Aneurysm Growth Evaluation and Detection (AGED): Comparison with Clinical Aneurysm Follow-Up.

Authors

Chien, Aichi
Špiclin, Žiga
Bizjak, Žiga
et al.

Publication Date

2022

Peer reviewed

HHS Public Access

Author manuscript

J Blood Disord Transfus. Author manuscript; available in PMC 2023 May 11.

Published in final edited form as:

J Blood Disord Transfus. 2022 ; 13(8): .

Computer-Assisted Aneurysm Growth Evaluation and Detection (AGED): Comparison with Clinical Aneurysm Follow-Up

Aichi Chien[a,*], **Žiga Špiclin**[b], **Žiga Bizjak**[b], **Kambiz Nael**[a]

[a]Department of Radiological Science, David Geffen School of Medicine at UCLA, 10833 LeConte Ave, Box 957350 Los Angeles, CA 90095

[b]University of Ljubljana, Faculty of Electrical Engineering Tržaška 25, SI-1000 Ljubljana, Slovenia

Abstract

Background and Purpose: Since growing intracranial aneurysms (IA) are more likely to rupture, detecting growth is an important part of unruptured IA follow-up. Recent studies have consistently shown that detecting IA growth can be challenging, especially in smaller aneurysms. In this study, we present an automated computational method to assist detecting aneurysm growth.

Materials and Methods: An analysis program, Aneurysm Growth Evaluation & Detection (AGED) based on IA images was developed. To verify the program can satisfactorily detect clinical aneurysm growth, we performed this comparative study using clinical determinations of growth during IA follow-up as a gold standard. Patients with unruptured, saccular IA followed by diagnostic brain CTA to monitor IA progression were reviewed. 48 IA image series from twenty longitudinally-followed ICA IA were analyzed using AGED. A set of IA morphologic features were calculated. Nonparametric statistical tests and ROC analysis were performed to evaluate the performance of each feature for growth detection.

Results: The set of automatically calculated morphologic features demonstrated comparable results to standard, manual clinical IA growth evaluation. Specifically, automatically calculated HMAX was superior (AUC = 0.958) at distinguishing growing and stable IA, followed by V, and SA (AUC = 0.927 and 0.917, respectively).

Conclusion: Our findings support automatic methods of detecting IA growth from sequential imaging studies as a useful adjunct to standard clinical assessment. AGED-generated growth detection shows promise for characterization and detection of IA growth and time-saving comparing with manual measurements.

Keywords

Unruptured intracranial aneurysms; Computer-assisted growth detection; Surface mesh reconstruction; Computed tomography angiography; Morphologic neuroimaging analysis

[*]Corresponding author Aichi Chien, PhD, Department of Radiological Science, David Geffen School of Medicine at UCLA, 10833 LeConte Ave, Box 957350 Los Angeles, CA 90095. aichi@ucla.edu.

Authors' contributions

All authors made substantial contributions to the conception or design of the work, acquisition, analysis, and interpretation of data, drafted and revised the work, approved the version to be published; and agree to be accountable for all aspects of the work in ensuring that questions related to the accuracy or integrity of any part of the work are appropriately investigated and resolved.

INTRODUCTION

The prevalence of unruptured intracranial aneurysms (IA) in the general population is estimated at 2 – 5 %, but the incidence of IA rupture and subarachnoid hemorrhage (SAH) is substantially lower, approximately 20 per 100,000 per year [1, 2]. IA treatment to prevent rupture has become increasingly safer with the widespread use of interventional approaches and intravascular devices. Since treating aneurysm remains expensive and not all unruptured IA will rupture, it is important to identify unruptured IA which need preventive treatment.

Current clinical practice leans towards preventative treatment for IA with diameter greater than 7 mm, and smaller IA which demonstrate growth, with exceptions made for conditions such as advanced patient age [3]. Therefore, for small unruptured IA, monitoring for interval growth through imaging follow-up is an important part of IA management. However, performing IA size measurements to detect growth can be a time-consuming task because small IA typically have proportionally small changes in size, and it may be necessary to check the IA from multiple angles. For example, a 10% increase in diameter for a 3 mm aneurysm would be growth of only 0.3 mm, whereas for a 6 mm aneurysm, a 10% increase would be 0.6 mm, significantly easier to detect. The reading time required to measure aneurysms during follow-up is often longer when the aneurysm is smaller.

Detecting IA growth is important. Past studies have linked IA growth to rupture [4]. A meta-analysis of 15 studies that investigated unruptured IAs and involved longitudinal monitoring using follow-up imaging found that the definition of size change measurements and associated growth thresholds varied substantially among studies [5]. For instance, size changes were characterized as changes in maximum dome diameter, maximum transverse dome diameter, increase in any dimension or increase in greatest diameter [6-11]. The assessment of growth was performed using manual measurement tools on 2D or 3D images and some included qualitative evaluation of IA shape and the appearance of blebs or lobes. To account for variations between manual measurements, different studies also have different growth thresholds, ranging from 0.5 to 2 mm. In spite of the variations in the growth detection threshold, these studies concluded that IA growth is highly correlated to rupture and have shed light on our understanding of the importance of detecting aneurysm growth. This knowledge has increased the number of unruptured IA followed through imaging. However, in the clinical setting, the technique to detect IA growth in follow-up images has remained comparison of multiple manual measurements.

In this research, we propose an automatic computational tool for aneurysm growth detection to provide quick, repeatable and consistent measurements. We present Aneurysm Growth Evaluation & Detection (AGED) to analyze aneurysm follow-up images. Our approach builds on methods to automatically define the IA neck and quantify IA morphologic characteristics [12]. We also utilize a shape morphing approach to automatically map the initial images and follow-up images and quantify differences. Clinical determinations of growth from those diagnostic IA images were set as the gold standard and compared with features automatically computed by AGED to verify their accuracy. The objective is to find the AGED features that detect growth accurately in a matter of seconds.

MATERIALS AND METHODS

Case information

This retrospective study was approved by the UCLA Institutional Review Board (UCLA IRB). This research was performed in accordance with relevant guidelines and regulations. As approved by the UCLA IRB for this retrospective study, informed consent was waived for all participants included in this research. Medical records for patients who had longitudinal imaging studies to monitor unruptured IA from 2005-2010 were reviewed. There were total of 235 patients who had unruptured IA followed by image studies during this period of time. For these patients, CTA follow-up image series were acquired with matrix size 512 x 512, field of view 180 mm, in-plane pixel size 0.39 mm, and section thickness 1.0 mm [4]. Among the follow-up IA cases, 180 were located at the ICA (18 growth, 162 stable), 56 ACA (6 growth, 50 stable), and 60 MCA (12 growth, 48 stable). To study the accuracy of automatic analysis by AGED and minimize potential bias due to case selection, IA from ICA locations with similar imaging interval were selected to provide balanced case numbers in the growth and stable groups.

Image processing and analysis

From each 3D CTA imaging study, the IA was manually located, and marching cubes and smooth non-shrinking algorithms were applied for segmentation and extraction of the IA and parent artery 3D surface mesh [13, 14]. Figure 1 shows the aligned initial and follow-up IA shapes separated by clinical growth/stable classification. Following segmentation, the surface mesh comprising the IA was isolated from the parent vessel using an automated cutting plane (ACP) method [12]. The isolated IA shape was used to compute the morphologic features. Morphologic features were computed using two general approaches. In the first approach, morphologic features were extracted directly using initial and follow-up IA meshes. Based on ACP methods, IA surface area (SA), volume (V), and maximum aneurysm dome size (HMAX) were calculated. Although similar to the manual clinical measurement of maximum diameter, because it is a computational analysis, HMAX effectively measures all possible directions in 3D to find the maximum distance in a fraction of a second. The relative change for each feature was computed by subtracting the initial and follow-up IA values: (follow-up value - initial value)/ initial value. The second approach was based on morphing calculations to estimate the path of IA growth from initial to follow-up. We implemented this morphing calculation to test if it provided better growth detection by considering the intermediate shapes between the initial and follow-up image (Figure 2). We utilized a two-stage morphing approach beginning with rigid alignment followed by non-rigid mesh-to-mesh deformation—to compute differential features including median deformation path length (dMPL), differential surface area (dSA), differential volume (dV), and differential integral of cumulative deformation distances (dICDD) [15]. The calculation of these morphologic features is illustrated and summarized in Figure 2.

Statistical analysis

For each feature, we computed the median and interquartile range (IQR). These are reported in the text in the format of median (IQR). To compare the groups, we used the non-parametric 2-sided Mann–Whitney U test, and to quantify the performance classifying

the cases we used the area under the curve (AUC) value computed from receiver operating characteristic (ROC) curve. For categorical variables, the 2-sided Chi-Square Test was used. Correlations were assessed using Kendall's tau-b. The statistical significance threshold was set as p-value < 0.01.

RESULTS

Table 1 summarizes the IA cases used in this study for comparative analysis. At initial imaging, recorded IA sizes were a median of 3.85 mm. The time interval between the initial scan and follow-up scans was a median of 2.5 years. To verify the study sample is unbiased, statistical analysis between groups was performed. Specifically, IA cases' anatomical locations, baseline sizes, and imaging intervals were not significantly different between groups. Patient characteristics, such as age at IA detection, family history of SAH, history of stroke or TIA, hypertension, thyroid disease, cancer, and atherosclerosis were also not significantly different between the groups. These results verify that the IA characteristics and patient characteristics were not different between groups when IA follow-up images were analyzed by clinical gold standard measurements. Therefore, using clinical gold standard follow-up IA measurements for these cases as a baseline comparison is appropriate to verify AGED accuracy in detecting IA growth in follow-up images.

Table 2 summarizes the IA growth analysis from clinical standard IA image measurements and results of different size related features computed by AGED. The analysis showed that AGED automatically computed features are comparable to gold-standard manual measurement for determining growth. The computer analysis shows promising results to detect growth specifically with automatically computed features using direct comparison between initial and follow-up IA images. Specifically, AGED using ACP analysis, the changes of HMAX, V, and SA showed promising results to detect growth ($p= 0.0002$, 0.001, and 0.001, respectively) (Table 2). According to ROC analysis, high classification scores of AUC = 0.958, 0.927, and 0.917 were achieved by HMAX, V, and SA, respectively (Table 2, Figure 3). With the AGED morphing analysis, only dSA, which estimates the expansion of the aneurysmal wall surface area, was statistically significant in detecting growth ($p<0.01$). However, according to ROC analysis, dSA had a relatively low AUC = 0.865 compared with features HMAX, V, and SA. Other features such as dMPL, dV, and dICDD were not able to statistically differentiate growth and stable IA ($p > 0.01$).

Figure 4 presents Tukey box-whisker plots of the clinical measurement for growth and stable groups and AGED automatically calculated morphologic values for different features. In general, higher values indicated growth for all factors except dICCD, including clinical size, HMAX, V, SA, dMPL, dV, and dSA. Overlap between the tails indicates a small degree of uncertainty when detecting growth, even with clinical size measurements. Taking the scale bar for each feature in Figure 4 into account, features computed with the morphing approach show greater overlap between stable and growth IA, suggesting they are not as efficient at detecting growth (differentiating growth and stable IAs).

DISCUSSION

Studies have shown the importance of monitoring aneurysm growth because growing aneurysms have higher risk of rupture. Many studies looking at IA growth practically focus on the prediction of growth. [3, 9, 16]. For example, Chien et al. reported the ability of IA volume, surface area, size ratio and NSI to predict growth. A recent retrospective study investigated various clinical scores (PHASES, UCAS, and ELAPSS) to predict IA growth [17]. Although these studies provide critical information to help identify IAs risk of growth and help high growth risk IAs to receive frequent follow-up to monitor growth, none of them address the challenge of detecting IA grow in clinical follow-up images. The current research presents an automatic computation to detect IA growth in follow-up images.

Currently, follow-up IA images need to be carefully compared with initial images, and clinical measurements and morphologic evaluation are commonly performed to detect growth for each IA. The AGED program is designed to follow clinical IA image follow-up measurement standards and use 3D analysis techniques to quickly detect growth based on computational methods. In the present study we found that many of the automated computed features—HMAX, V, SA and dSA—had comparable performance to the standard clinical measurements to detect growth. Specifically, HMAX provided superior accuracy in growth evaluation. This is likely because the feature HMAX computes maximum distance in 3D IA images similarly to the clinical standard. It should be noted that HMAX is an automated, objective assessment and is generated within a fraction of a second. Implementing HMAX may be a useful addition to clinical IA evaluation while clinicians perform critical review of aneurysm blebs or irregular shapes.

In this study we employed the longitudinal IA shape ACP and morphing analysis methods to calculate various IA growth-related features. Shape morphing deforms the IA surface mesh extracted from the initial scan into the shape extracted from the follow-up scan. The result of shape morphing is a deformation field that maps how the baseline shape develops into the follow-up one. We found stronger correlation between the method of feature computation (SA and V (0.947, $p<0.01$), dSA and dV (0.821, $p<0.01$)) than the corresponding features (SA and dSA (0.474, $p<0.01$), V and dV (0.389, $p=0.016$)). Thus, we found that the computational method affected how well the features detect growth. This further suggests that the change in surface area calculated with the morphing approach (dSA) may differ from that calculated by comparing surface area directly (SA). Since the morphing analysis assumes the surface mesh changes under a mathematical function, further study to investigate the relationship between SA and dSA with longer follow-up time may be useful to understand whether there are local IA wall changes (such as bleb formation) which challenge the morphing approach. In such a case, the resulting morphing-estimated IA surface wall change may be smaller than the actual wall change. Localized or regional changes in IA wall during growth are known to occur related to hemodynamics or local wall damage [18]. Differences between the calculation methods may indicate specific local wall damage which has weakened the wall and caused certain regions to grow at a different rate.

The AGED morphing approach to identify changes in follow-up images is relatively new to IA, but similar techniques have been previously applied to other biological problems

[19, 20]. In this study we compared two novel features that characterize the deformation field, the first being median deformation path length normalized by baseline aneurysm size (dMPL), and second the integral of cumulative deformation distances (dICDD). Likely due to these features simplifying the complex deformation field to a single value, these two features did not show satisfactory performance to detect growth. dMPL and dICDD is to analyze small changes in the growth path, further improvement of these feature analyses for specific regions of IA growth may provide new information related to regional growth characteristics and the details of IA growth [15].

LIMITATIONS

The main challenges for detecting IA growth are the imaging resolution and the size of IA being followed, which is typically small. Therefore, the technique to detect growth needs to be robust to consistently find changes between initial IA images and follow-up IA. We studied a group of IA with clinical follow-up studies to verify the ability of AGED to detect IA growth is comparable to clinical measurements. Additional study with longer follow-up and testing more IA in various anatomical locations can further verify the program accuracy and evaluate performance of different features.

CONCLUSION

We applied a computational approach for detection of morphologic changes in unruptured IA. Morphologic features computed from longitudinal image studies provided automated results comparable to current clinical assessment of IA growth. The algorithms we developed were compared with clinical standard, manual measurements and demonstrated satisfactory performance to detect growth (AUC = 0.958).

Funding

This research was supported in part by NIH NHLBI R01HL152270

Abbreviations:

AGED	Aneurysm Growth Evaluation & Detection program
AUC	area under the receiver operating characteristic curve
HMAX	maximum aneurysm dome size
dMPL	differential median deformation path length
dSA	differential surface area
dV	differential volume
dICDD	differential integral of cumulative deformation distances
IA	intracranial aneurysm
IQR	interquartile range

ROC	receiver operating characteristic
SAH	subarachnoid hemorrhage

REFERENCES

1. Vlak MH, Algra A, Brandenburg R, Rinkel GJ. Prevalence of unruptured intracranial aneurysms, with emphasis on sex, age, comorbidity, country, and time period: a systematic review and meta-analysis. The Lancet Neurology 2011;10:626–636. [PubMed: 21641282]
2. Kotowski M, Naggara O, Darsaut TE, et al. Safety and occlusion rates of surgical treatment of unruptured intracranial aneurysms: a systematic review and meta-analysis of the literature from 1990 to 2011. Journal of Neurology, Neurosurgery & Psychiatry 2013;84:42–48. [PubMed: 23012447]
3. Thompson BG, Brown RD Jr., Amin-Hanjani S, et al. Guidelines for the Management of Patients With Unruptured Intracranial Aneurysms: A Guideline for Healthcare Professionals From the American Heart Association/American Stroke Association. Stroke 2015;46:2368–2400. [PubMed: 26089327]
4. Villablanca JP, Duckwiler GR, Jahan R, et al. Natural History of Asymptomatic Unruptured Cerebral Aneurysms Evaluated at CT Angiography: Growth and Rupture Incidence and Correlation with Epidemiologic Risk Factors. Radiology 2013;269:258–265. [PubMed: 23821755]
5. Daan B, J.E. RG, LK G, Ale A, D.I. VM. Patient- and Aneurysm-Specific Risk Factors for Intracranial Aneurysm Growth. Stroke 2016;47:951–957. [PubMed: 26906920]
6. Matsubara S, Hadeishi H, Suzuki A, Yasui N, Nishimura H. Incidence and risk factors for the growth of unruptured cerebral aneurysms: observation using serial computerized tomography angiography. Journal of Neurosurgery 2004;101:908–914. [PubMed: 15597749]
7. Juvela S, Poussa K, Porras MAN. Factors affecting formation and growth of intracranial aneurysms: a long-term follow-up study. Stroke 2001;32:485–491. [PubMed: 11157187]
8. Matsumoto K, Oshino S, Sasaki M, Tsuruzono K, Taketsuna S, Yoshimine T. Incidence of growth and rupture of unruptured intracranial aneurysms followed by serial MRA. Acta Neurochirurgica 2013;155:211–216. [PubMed: 23196925]
9. Ferns SP, Sprengers ME, van Rooij WJ, et al. De novo aneurysm formation and growth of untreated aneurysms: a 5-year MRA follow-up in a large cohort of patients with coiled aneurysms and review of the literature. Stroke 2011;42:313–318. [PubMed: 21164110]
10. Burns JD, Huston J 3rd, Layton KF, Piepgras DG, Brown RD Jr. Intracranial aneurysm enlargement on serial magnetic resonance angiography: frequency and risk factors. Stroke 2009;40:406–411. [PubMed: 19023101]
11. Phan TG, Huston J 3rd, Brown RD Jr., Wiebers DO, Piepgras DG. Intracranial saccular aneurysm enlargement determined using serial magnetic resonance angiography. J Neurosurg 2002;97:1023–1028. [PubMed: 12450022]
12. Jerman T, Pernuš F, Likar B, Špiclin Ž, Chien A. Automatic cutting plane identification for computer-aided analysis of intracranial aneurysms. 2016 23rd International Conference on Pattern Recognition (ICPR); 2016 December 2016: 1484–1489.
13. Cebral JR, Löhner R. From medical images to anatomically accurate finite element grids. International Journal for Numerical Methods in Engineering 2001;51:985–1008.
14. Lorensen WE, Cline HE. Marching Cubes: A High Resolution 3D Surface Construction Algorithm. 1987 1987: ACM: 163–169.
15. Bizjak Ž, Jerman T, Likar B, Pernuš F, Chien A, Špiclin Ž. Registration based detection and quantification of intracranial aneurysm growth. Medical Imaging 2019: Computer-Aided Diagnosis; 2019 2019/03/13: International Society for Optics and Photonics: 1095007.
16. Chien A, Xu M, Yokota H, Scalzo F, Morimoto E, Salamon N. Nonsphericity Index and Size Ratio Identify Morphologic Differences between Growing and Stable Aneurysms in a Longitudinal Study of 93 Cases. American Journal of Neuroradiology 2018;39:500–506. [PubMed: 29371255]

17. Sturiale CL, Stumpo V, Ricciardi L, et al. Retrospective application of risk scores to ruptured intracranial aneurysms: would they have predicted the risk of bleeding? Neurosurgical review 2021;44:1655–1663. [PubMed: 32715359]

18. Nordahl ER, Uthamaraj S, Dennis KD, et al. Morphological and Hemodynamic Changes during Cerebral Aneurysm Growth. Brain sciences 2021;11. [PubMed: 35053755]

19. Yushkevich PA, Aly A, Wang J, et al. Diffeomorphic Medial Modeling. Information processing in medical imaging : proceedings of the conference 2019;11492:208–220. [PubMed: 32410804]

20. Bône A, Colliot O, Durrleman S. Learning the spatio-temporal variability of longitudinal shape data sets: application to Alzheimer's disease progression modeling. 2019.

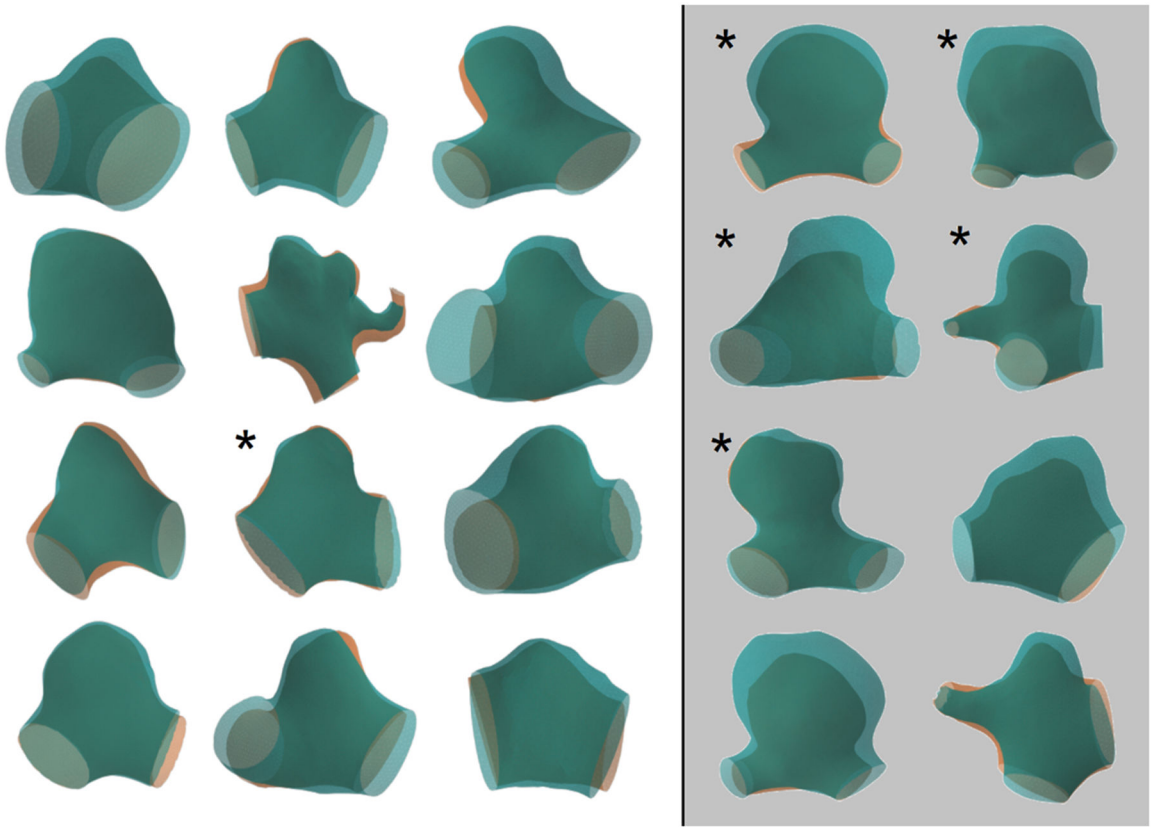

Figure 1:
3D reconstructions of IA based on initial images (*orange*) and follow-up images (*green*) shapes. Based on clinical IA follow-up measurements, stable IAs are shown on the left and growing IAs are shown on the right. Asterisks mark aneurysms treated at some point after the follow-up imaging.

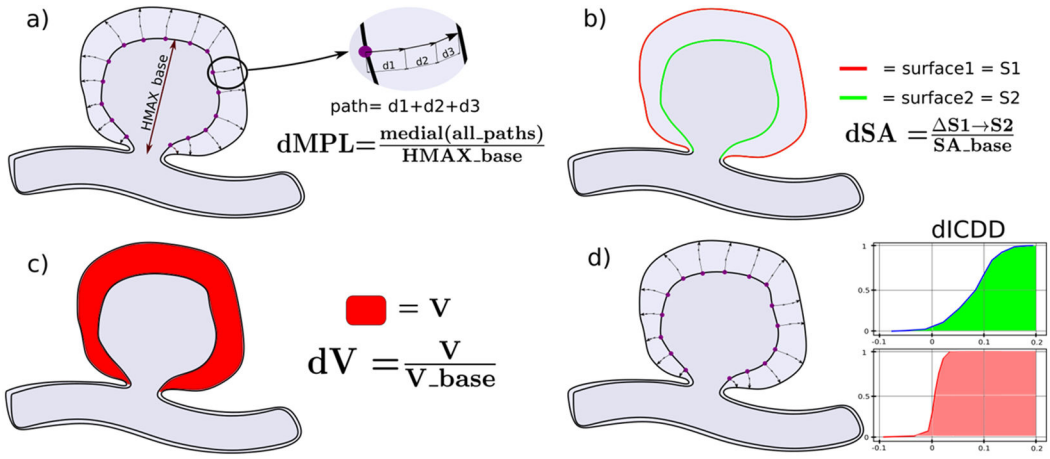

Figure 2:

Graphic presentation of four novel features for AGED morphing analysis to quantify IA changes: a) differential median deformation path length (dMPL), accumulates the deformation paths of all vertices that represent the initial IA shape, normalized by dividing by initial HMAX . b) differential surface area (dSA), surface change between deformed and initial IA dome surface mesh divided by initial IA dome surface mesh. c) differential volume (dV), volume changes between deformed and initial IA divided by initial IA volume. d) differential integral of cumulative deformation distances (dICCD), area under the curve of cumulative distribution function of growth paths.

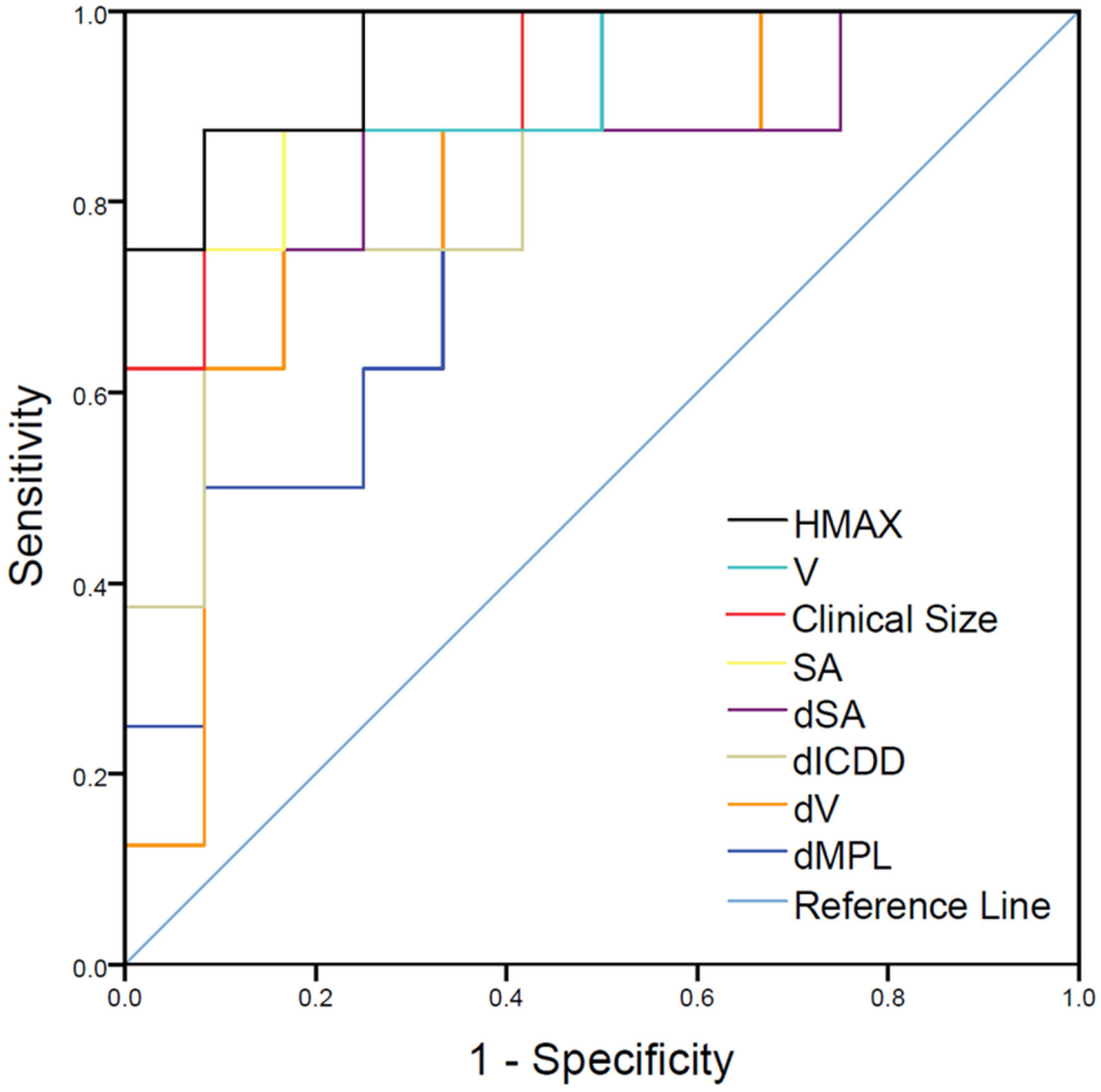

Figure 3.
ROC Curve for features for classification of IA growth relative to clinical determination. AUC are values provided in Table 2.

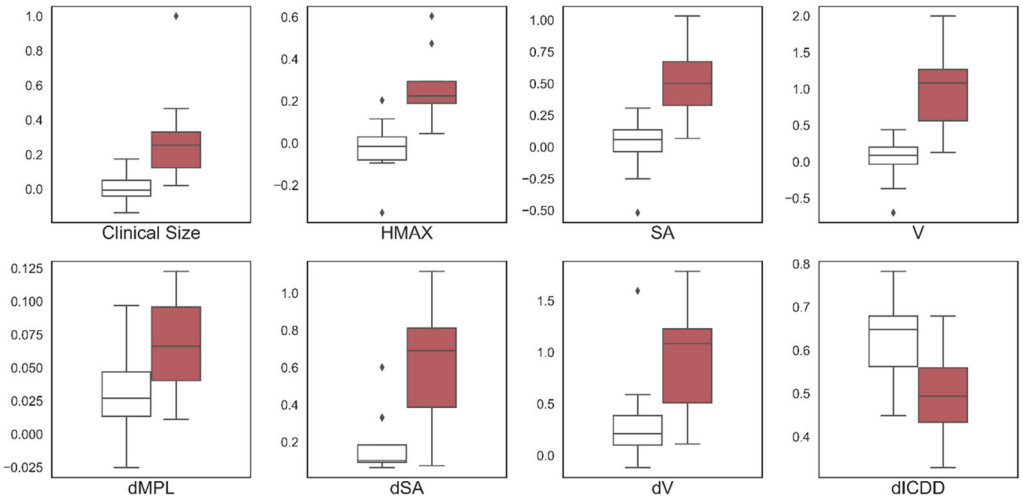

Figure 4:

Tukey box-whisker plots for the stable (white) and growing (red) IA groups and morphologic features. Outliers are indicated with diamonds. Features are presented as changes normalized with respect to value obtained from initial IA. HMAX, V, and SA obtained from ACP approach and dMPL, dSA, dV and dICDD obtained by morphing approach.

Table 1:

Summary of the IA cases included in this study to verify AGED against gold standard clinical IA growth evaluation.

	Total	Stable	Growth
Number of Patients	20	12	8
Patient Age (years)	69.8 (16.2)	68.5 (17.2)	69.8 (14.7)
Imaging Interval (years)	2.50 (2.75)	2.50 (4.75)	2.50 (1.0)
Initial image aneurysm Size (mm)	3.85 (4.30)	3.45 (3.95)	6.15 (6.25)
FU Max Size (mm)	6.10 (7.38)	3.85 (3.63)	8.40 (8.08)
IA Treated	6	1	5
Aneurysm Location			
ICA-Posterior Communicating Artery	6	2	4
ICA-Superior Hypophyseal Artery	10	6	4
ICA-Ophthalmic Artery	4	4	0
Family History of SAH	1	1	0
Stroke or TIA	3	1	2
Hypertension	9	5	4
History of Smoking	3	3	0
Thyroid Disease	2	2	0
Cancer	4	2	2
Atherosclerosis	13	9	4

Results are presented as median and interquartile range, Median (IQR)

Table 2.

Statistical differences between IA identified as growing and stable. Each feature represents the normalized change between the two imaging points.

	Stable IA	Growth IA	Mann-Whitney *U* statistic	Mann-Whitney *U* Significance (p)	ROC Area Under the Curve
Clinical measurements	−0.005 (0.094)	0.254 (0.340)	85	0.007	0.927
HMAX	−.016 (0.167)	0.224 (0.264)	92	**0.0002**	**0.958**
V	0.087 (0.360)	1.07 (1.09)	89	**0.001**	**0.927**
SA	0.056 (0.240)	0.501 (0.480)	88	**0.001**	**0.917**
dMPL	0.027 (0.041)	0.066 (0.068)	74	0.047	0.771
dSA	0.100 (0.206)	0.691 (0.522)	83	**0.005**	0.865
dV	0.211 (0.407)	1.08 (1.03)	78	0.020	0.812
dICDD	0.648 (0.120)	0.494 (0.165)	17	0.016	0.823

Results are presented as median and interquartile range, Median (IQR)